Biomed Microdevices (2014) 16:793–804
DOI 10.1007/s10544-014-9883-z

Bicomponent electrospinning to fabricate three-dimensional hydrogel-hybrid nanofibrous scaffolds with spatial fiber tortuosity

Gyuhyung Jin · Slgirim Lee · Seung-Hyun Kim · Minhee Kim · Jae-Hyung Jang

Published online: 28 June 2014
© Springer Science+Business Media New York 2014

Abstract Electrospun fibrous mats have emerged as powerful tissue engineering scaffolds capable of providing highly effective and versatile physical guidance, mimicking the extracellular environment. However, electrospinning typically produces a sheet-like structure, which is a major limitation associated with current electrospinning technologies. To address this challenge, highly porous, volumetric hydrogel-hybrid fibrous scaffolds were fabricated by one Taylor cone-based side-by-side dual electrospinning of poly (ε-caprolactone) (PCL) and poly (vinyl pyrrolidone) (PVP), which possess distinct properties (*i.e.*, hydrophobic and hydrogel properties, respectively). Immersion of the resulting scaffolds in water induced spatial tortuosity of the hydrogel PVP fibers while maintaining their aligned fibrous structures in parallel with the PCL fibers. The resulting conformational changes in the entire bicomponent fibers upon immersion in water led to volumetric expansion of the fibrous scaffolds. The spatial fiber tortuosity significantly increased the pore volumes of electrospun fibrous mats and dramatically promoted cellular infiltration into the scaffold interior both *in vitro* and *in vivo*. Harmonizing the flexible PCL fibers with the soft PVP-hydrogel layers produced highly ductile fibrous structures that could mechanically resist cellular contractile forces upon *in vivo* implantation. This facile dual electrospinning followed by the spatial fiber tortuosity for fabricating three-dimensional hydrogel-hybrid fibrous scaffolds will extend the use of electrospun fibers toward various tissue engineering applications.

Keywords Spatial fiber tortuosity · Tissue engineering scaffolds · Three dimensional fibers · Electrospinning · Hybrid

1 Introduction

Orchestrating extracellular environments is crucial when mediating tissue morphogenesis in the body (De Laporte and Shea 2007). In tissue engineering approaches, designing scaffolds that can mimic the structural and functional aspects of the extracellular matrix (ECM) can be highly beneficial for organizing new tissue formation (Howard et al. 2008). Therefore, electrospun non-woven fibrous mats fabricated under a high electric field have received significant attention as scaffolds for tissue engineering due to their structural similarity to the natural ECM (Doshi and Reneker 1995; Agarwal et al. 2009). Moreover, their additional advantageous characteristics, including their high surface-to-volume ratio, ease of processing, easy functionalization, and various topographical features, have enabled extensive utilization in numerous tissue engineering applications (Agarwal et al. 2009; Nisbet et al. 2009): smooth muscle (Nivison-Smith et al. 2012), skeletal muscle (Chen et al. 2013), bone (Phipps et al. 2012), cartilage (Xue et al. 2013), skin (Kim et al. 2012), cardiac (Kharaziha et al. 2013), and neural tissue regeneration (Ren et al. 2013). However, the highly dense accumulation of nanofibers obtained by electrospinning typically results in two-dimensional sheet-like structures, which limits cellular infiltration (Nisbet et al. 2009). Therefore, designing novel electrospun fibrous scaffolds that address these structural challenges will expand the utility of these materials in various tissue engineering applications.

Gyuhyung Jin and Slgirim Lee are contributed equally

Electronic supplementary material The online version of this article (doi:10.1007/s10544-014-9883-z) contains supplementary material, which is available to authorized users.

G. Jin · S. Lee · S.-H. Kim · M. Kim · J.-H. Jang (✉)
Department of Chemical and Biomolecular Engineering, Yonsei University, 50 Yonsei-Ro, Seoul 120-749, South Korea
e-mail: j-jang@yonsei.ac.kr

Numerous efforts have been made to design three-dimensional electrospun scaffolds. When including porogens in electrospun fibers during the fabrication process, the porosities of the scaffolds were expanded, ultimately improving cellular infiltration into the scaffolds (Lee et al. 2005; Nam et al. 2007; Kim et al. 2008; Wang et al. 2009). Introducing and then removing water-soluble sacrificial fibers, such as poly (ethylene oxide) fibers, has also provided volumetric flexibility in electrospun scaffolds (Baker et al. 2008; Ekaputra et al. 2008; Shin et al. 2009; Whited et al. 2011; Phipps et al. 2012). The repulsion between electrospun nanofibers under a strong electric field has been used to generate fluffy fibrous scaffolds (Sun et al. 2012; Lee et al. 2014). Additionally, UV irradiation (Yixiang et al. 2008; Sundararaghavan et al. 2010), the addition of chemical blowing agents (Kim et al. 2007), the incorporation of hyaluronan (Li et al. 2012), and the deposition of a glycosaminoglycan hydrogel (Ekaputra et al. 2008) have been suggested for achieving large pore sizes and improving cellular ingrowth. Furthermore, modified collectors, such as patterned (Vaquette and Cooper-White 2011) or bowl-like collectors with metallic needles (Blakeney et al. 2011), have been utilized to produce three-dimensional electrospun fibrous structures. Various modifications to the electrospinning process, such as combination electrospinning of nano- and micro-fibers (Pham et al. 2006; Thorvaldsson et al. 2008), cryogenic electrospinning (Leong et al. 2009), wet electrospinning (Jiao et al. 2006; Ki et al. 2007), and light emission array electrospinning (Shabani et al. 2012), have also been employed to address the structural challenges of electrospinning. Additionally, hydrogel materials have been employed in electrospinning to enhance cellular penetration into the interior areas of scaffolds (Ekaputra et al. 2008; Li et al. 2012), formulate three-dimensional structures (Ji et al. 2006), and improve mechanical properties (Thorvaldsson et al. 2013; Strange et al. 2014).

In this study, a facile side-by-side dual electrospinning technique using a one Taylor cone system, which was adopted from previous studies (Gupta and Wilkes 2003; Zhu et al. 2013), has been employed to fabricate three-dimensional hydrogel-hybrid fibrous scaffolds. Two polymers, poly (ε-caprolactone) (PCL) and poly (vinyl pyrrolidone) (PVP), which possess distinct characteristic properties (*i.e.*, hydrophobicity vs. hydrogel), were electrospun in parallel using a custom designed dual nozzle. Due to its solubility in various organic solvents, biocompatibility, and hydrophilicity, PVP has previously been used as a carrier for drug delivery or as a blending material for electrospun fibers (Jiao et al. 2006; Xu et al. 2009; Jia et al. 2011; Kim et al. 2013; Lee et al. 2013). Importantly, PVP can be easily crosslinked using 4,4′-diazidostilbene-2,2′-disulfonic acid disodium salt (DAS) and UV irradiation, imparting a swelling property (Ignatova et al. 2007). The PCL fibers played a pivotal role for sustaining the three-dimensional frame of newly expanded electrospun scaffolds and also inducing three-dimensional curvature of the PVP fibers. Except for aligning two nozzles in parallel to form one Taylor cone prior to electrospinning, no additional or complicated equipment was required to form the three-dimensional hydrogel-hybrid fibrous structures. Most importantly, fibrous structures of the hydrogel-hybrid scaffolds were maintained after swelling, and a spatial fiber tortuosity upon immersion in water played a key role in expanding the volume of the PCL-PVP hydrogel-hybrid fibrous scaffolds. The resulting fibrous scaffolds were characterized *in vitro* and *in vivo* to reveal their potential for use in tissue engineering applications. This unique electrospinning technique addresses the structural limitations of conventional electrospun scaffolds, advancing the technique of electrospinning and potentially enabling its extensive use in numerous tissue engineering applications.

2 Materials and methods

2.1 Fabrication of side-by-side hydrogel-hybrid fibrous scaffolds

Three-dimensional hydrogel-hybrid fibrous scaffolds composed of two polymers with distinct properties were fabricated using an electrospinning system (ESR 100, NanoNC, Seoul, Korea) with a custom dual nozzle, as shown in Fig. 1a and b. The nozzle was designed to align two needles (23G, inner diameter=330.0 μm) in parallel for the simultaneous extrusion of two polymer solutions side by side. Briefly, poly (ε-caprolactone) (PCL) (average molecular weight 80,000 g/mol: Sigma-Aldrich, St. Louis, MO, USA) was dissolved in a mixture comprising chloroform (99.0 %, Duksan Pure Chemicals, Ansan, Korea) and N,N-dimethylformamide (DMF) (99.9 %, Duksan Pure Chemicals) (v/v ratio=4:1) to prepare a 15 % (w/v) solution. Similarly, PVP (average molecular weight 360,000 g/mol: Sigma-Aldrich) was dissolved in ethyl alcohol (99.9 %, Duksan Pure Chemicals) to prepare a 15 % (w/v) solution. Simultaneous electrospinning of the PCL and PVP solutions from the dual nozzle was conducted under a high voltage (12 kV, working distance 12 cm), and the feed rates of each nozzle were varied (PCL: PVP=2.0:0.0, 1.4:0.6, 1.0:1.0, 0.6:1.4, and 0.0:2.0 mL/h) to formulate various PVP compositions within the resulting scaffolds (*i.e.*, 0, 30, 50, 70, and 100 % (v/v)) (Table 1). Prior to electrospinning, 0.03 % (w/w) 4,4′-diazidostilbene-2,2′-disulfonic acid disodium salt (DAS) (Tokyo Kasei Kogyo, Tokyo, Japan) was introduced to the PVP solution. The electrospun fibers were exposed to UV light (INNO-CURE 100 N, Lichtzen, Ansan, Korea) to induce the photo-crosslinking of PVP fibers. The resulting fibrous scaffolds, which consisted of flat fibers, were collected on aluminum foil for 1 hour and dried at room temperature to remove any solvent. Subsequently, each scaffold, which

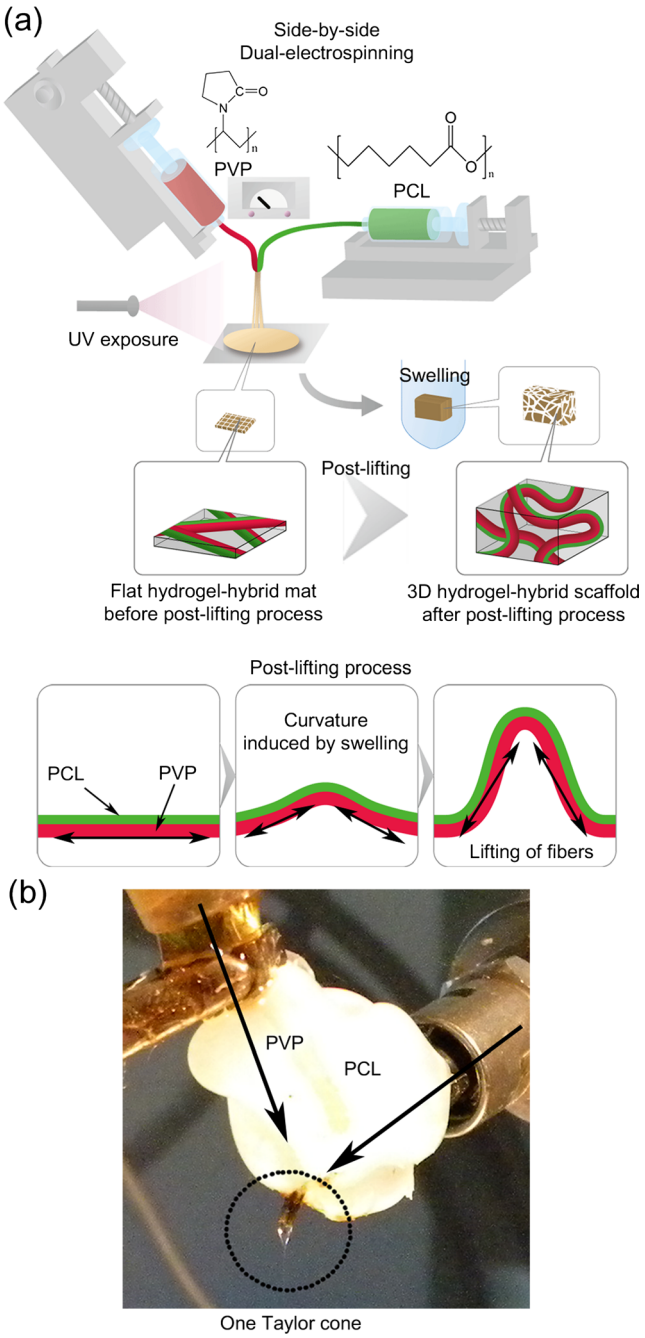

Fig. 1 Schematic illustration (**a**) and a custom designed dual nozzle (**b**) depicting the 'spatial fiber tortuosity,' which consisted of side-by-side dual electrospinning of different materials using two aligned nozzles under UV irradiation, followed by swelling. The *dotted line* in (**b**) illustrates the one Taylor cone generated from the dual nozzle. The electrospun fibers, composed of PVP and PCL fibers, were exposed to UV spots during the process and immersed in water to swell the PVP fibers. The swollen PVP portions volumetrically expanded the hydrogel-hybrid fibrous structures

contained varying quantities of PVP, was immersed in deionized water for 24 hours to eliminate any residual uncrosslinked PVP polymers, increasing the volume of the PCL-PVP scaffold.

Table 1 Experimental parameters and abbreviations for each scaffold setup

Volumetric ratio (PCL: PVP)	Feed rate (mL/h)		Abbreviation	Electrospinning setup
	PCL	PVP		
100:0	2	0	PCL100	Single ejecting
70:30	1.4	0.6	PCL_PVP30	Side-by-side/dual
50:50	1	1	PCL_PVP50	Side-by-side/dual
30:70	0.6	1.4	PCL_PVP70	Side-by-side/dual
0:100	0	2	PVP100	Single ejecting

2.2 Characterization of the hydrogel-hybrid scaffolds

The physical and chemical characteristics of the resulting fibrous scaffolds were determined by analyzing the fiber morphology, mechanical strength, and chemical composition. The morphology of the fibrous structures was visualized using field emission scanning electron microscopy (FE-SEM) (JEOL-7001 F, JEOL Ltd., Tokyo, Japan) at 15 kV. The diameters of swollen-electrospun fibers, which were randomly selected from the SEM images, were measured using Image J software (NIH, Bethesda, MD, USA). To visualize the fibrous non-swollen structures by fluorescence microscopy, coumarin (Sigma-Aldrich) and rhodamine B (Sigma-Aldrich) were added to the PCL and PVP solutions or vice versa at a concentration of approximately 0.01 % (w/v) prior to electrospinning. The images of individual fibers containing either coumarin or rhodamine B before and after swelling were then acquired by confocal laser scanning microscopy (CLSM, LSM 700, Carl Zeiss, Thornwood, NY, USA). The mechanical properties of the fibrous scaffolds before and after swelling were characterized by investigating the stress–strain behaviors of the resulting scaffolds, measured using a universal testing machine (Multi Test 1-i, Mecnnesin, Slinfold, UK) equipped with a 50 N load cell at a fixed loading rate (19 mm/min). The dimensions of the test specimens were 4.320±1.028 mm width and 0.602±0.728 mm depth, measured with a micrometer (IP 65, Mitutoyo, Kanagawa, Japan). The composition of the PCL-PVP composite scaffolds fabricated by varying the quantity of PVP within the scaffold was characterized by Fourier transform infrared (FT-IR) spectroscopy (Spectrum 100, Perkin Elmer, Waltham, MA, USA). The swelling ratio of the scaffolds was analyzed by measuring the dimensions after swelling with a micrometer. To determine the porosity of each scaffold, the volume of pores per unit mass of scaffold, called the specific pore volume (cm^3/g), was calculated using the following equation (Cai et al. 2013):

$$V_{sp} = \frac{V_{pore}}{m_{scaffold}} = \frac{V_{scaffold}}{m_{scaffold}} - \frac{1}{\rho_{material}}$$

where V_{pore} is the volume of pores, $m_{scaffold}$ is the mass of the scaffold, $V_{scaffold}$ is the volume of the scaffold, and $\rho_{material}$ is the theoretical density of the PCL-PVP composite (PCL:1.145 g/cm^3, PVP:1.2 g/cm^3), calculated according to the volumetric ratio.

2.3 Cell seeding and culture

Cellular infiltration into the swollen PCL-PVP hydrogel-hybrid nanofibrous scaffolds was investigated using the NIH3T3 cell line derived from mouse fibroblasts. The cells were cultured in Dulbecco's modified Eagle's medium (DMEM; Invitrogen, Carlsbad, CA, USA) supplemented with 10 % fetal bovine serum (FBS) (Invitrogen) and 1 % penicillin and streptomycin (Invitrogen) at 37 °C and 5 % CO_2. Prior to cell seeding, the electrospun scaffolds were immersed in 70 % ethanol for 30 minutes for sterilization, transferred to deionized water for 24 hours, and finally transferred to DMEM/10 % FBS that was stored at 37 °C overnight. The adsorption of the serum components (*e.g.*, fibronectin) facilitates cellular adhesion on the synthetic polymer surfaces (Jang et al. 2006). The scaffolds were placed in a 96-well tissue culture plate (TCP) and air-dried for 5 minutes at room temperature to remove some of the moisture from the inner space of the scaffolds. Subsequently, NIH3T3 cell suspensions (7×10^4 cells/scaffold) were pipetted on top of the scaffolds, and the cell-seeded scaffolds were incubated for 2 hours to allow the cells to attach to the surface. Finally, additional medium (200 μL) was added to the wells containing scaffolds, and the medium was replaced with fresh medium every day until analysis.

2.4 *In vitro* characterization of the hydrogel-hybrid scaffolds

The viability of the NIH3T3 cells grown within the PCL-PVP hydrogel-hybrid fibrous scaffolds was determined using a WST-1 cell cytotoxicity assay kit (Roche Applied Science, Indianapolis, IN, USA) according to the manufacturer's protocol. Briefly, at 3 and 7 days post-culture, 20 μL of a WST-1 solution was added directly into the 200 μL of medium containing the scaffolds, and the colorimetric change of the supernatant at 440 nm was measured using a spectrophotometer (Nanodrop 2000, Thermo Scientific, West Palm Beach, FL, USA). Additionally, cellular infiltration into the inner space of the scaffolds was assessed. At 7 days post-culture, the cells within each scaffold were fixed in 4 % paraformaldehyde (PFA) overnight at 4 °C. Subsequently, the fixed cell-scaffold blocks were frozen in optical cutting temperature compound (OCT) at −80 °C and cut into 16-μm thick sections using a cryostat microtome (Leica, CM1850, Leica Biosystems, Wetzlar, Germany). The sections were then stained with hematoxylin and eosin (H&E; Sigma-Aldrich) and observed under bright-field microscopy (Nikon Eclipse Ti, Nikon Corporation, Tokyo, Japan) to examine the cellular distribution within the scaffolds. The cells within the scaffold interior were visualized by staining with Hoechst dye (Hoechst 33258; Sigma-Aldrich). The morphologies of the cells on each scaffold, which were fixed by 2.5 % glutaraldehyde, were also visualized using FE-SEM.

2.5 *In vivo* characterization of hydrogel-hybrid fibrous scaffolds

To investigate both the *in vivo* cellular infiltration across the scaffold interior and the mechanical integrity of the swollen PCL-PVP composite scaffolds, the flat PCL-only scaffolds or PCL_PVP50 scaffolds were implanted subcutaneously into female C57BL/6 mice (20–22 g; n=3). All of the experimental procedures followed the guidelines for the care and handling of laboratory animals and were approved by the Yonsei Laboratory Animal Research Center Institutional Animal Care and Use Committee (YLARC-IACUC, Yonsei University, Korea). The scaffolds were retrieved at 7 days post-implantation and fixed in 4 % PFA overnight at 4 °C. Tissue sections frozen in OCT were cut into 16-μm thick sections using a cryostat microtome and stained with H&E to assess both the cellular distribution within the implanted scaffolds and the mechanical integrity of the scaffolds against cellular contractile forces.

2.6 Statistical analysis

All statistical analyses were performed using a one-way analysis of variance (ANOVA) with a *post hoc* Dunnett's test in the SPSS (Statistical Package for the Social Sciences) 21.0 software package (IBM Corporation, Somers, NY, USA).

3 Results and discussion

Simultaneous electrospinning of PCL and PVP using a custom designed dual nozzle under UV irradiation followed by immersion in deionized water (Fig. 1a) generated highly porous three-dimensional hydrogel-hybrid fibrous scaffolds. As shown in Fig. 1b, an additional needle was installed along with an original one to allow for the ejection of both fibers side-by-side. If the differences in conductivity between two aligned polymers under a high electric field are significant, electrostatic repulsion can cause separation of the two aligned polymers upon ejection (Gupta and Wilkes 2003). To resolve this issue, one Taylor cone was generated to eject stable jets from the dual nozzle (Fig. 1b). The volumetric ratio of the PCL and PVP polymers within the fibrous scaffolds, which were dissolved in a solvent mixture (chloroform: N,N-dimethyl formamide (DMF)=4:1, v/v) and ethyl alcohol, respectively,

was regulated by varying the feed rates of each polymer solution from each nozzle. Table 1 presents the abbreviations for each scaffold setup and the experimental parameters, including the volumetric ratio and feed rates.

Dramatic morphological changes in the side-by-side electrospun fibers containing PVP fibers (*i.e.*, PCL_PVP30, PCL_PVP50, PCL_PVP70, and PVP100) crosslinked under UV irradiation were observed after immersion in deionized water (Fig. 2a). The digits in the abbreviations of the scaffold formulations indicate the volumetric proportion of PVP in the fibrous scaffolds (Table 1). Importantly, formulating core-sheath PCL-PVP structures or electrospinning a blended PCL-PVP solution did not generate substantial volumetric expansion compared to the side-by-side dual electrospinning approach (Online Resource 1). When the PVP layers were fully covered or blended with the hydrophobic PCL layers (Online Resource 2), the contact area of the PVP chains that could interact with moisture for hydrogelation was likely much smaller than when the PVP layers were fully exposed along with the PCL (*i.e.*, side-by-side dual electrospinning). Additionally, when a shell layer was formulated with PVP (Online Resource 2), the extent of the conformational changes of the thin outer PVP layer, which symmetrically covered PCL fibers, was likely smaller than those of PVP fibers that asymmetrically wrapped or were aligned side-by-side with PCL fibers. Taken together, the core-sheath structures or blended mats appear to elicit smaller driving forces to result in the tortuosity of fibers compared to side-by-side dual electrospinning. Therefore, to maximize the spatial fiber tortuosity upon immersion in water, further analysis was conducted using the side-by-side dual electrospinning. Exposure of PVP-containing scaffolds to UV light induced a color change to dark-brown, indicating PVP-crosslinking with 4,4′-diazidostilbene-2,2′-disulfonic acid disodium salt (DAS) (Ignatova et al. 2007). After immersion in water, remarkable changes in the thickness of PVP-containing fibrous scaffolds,

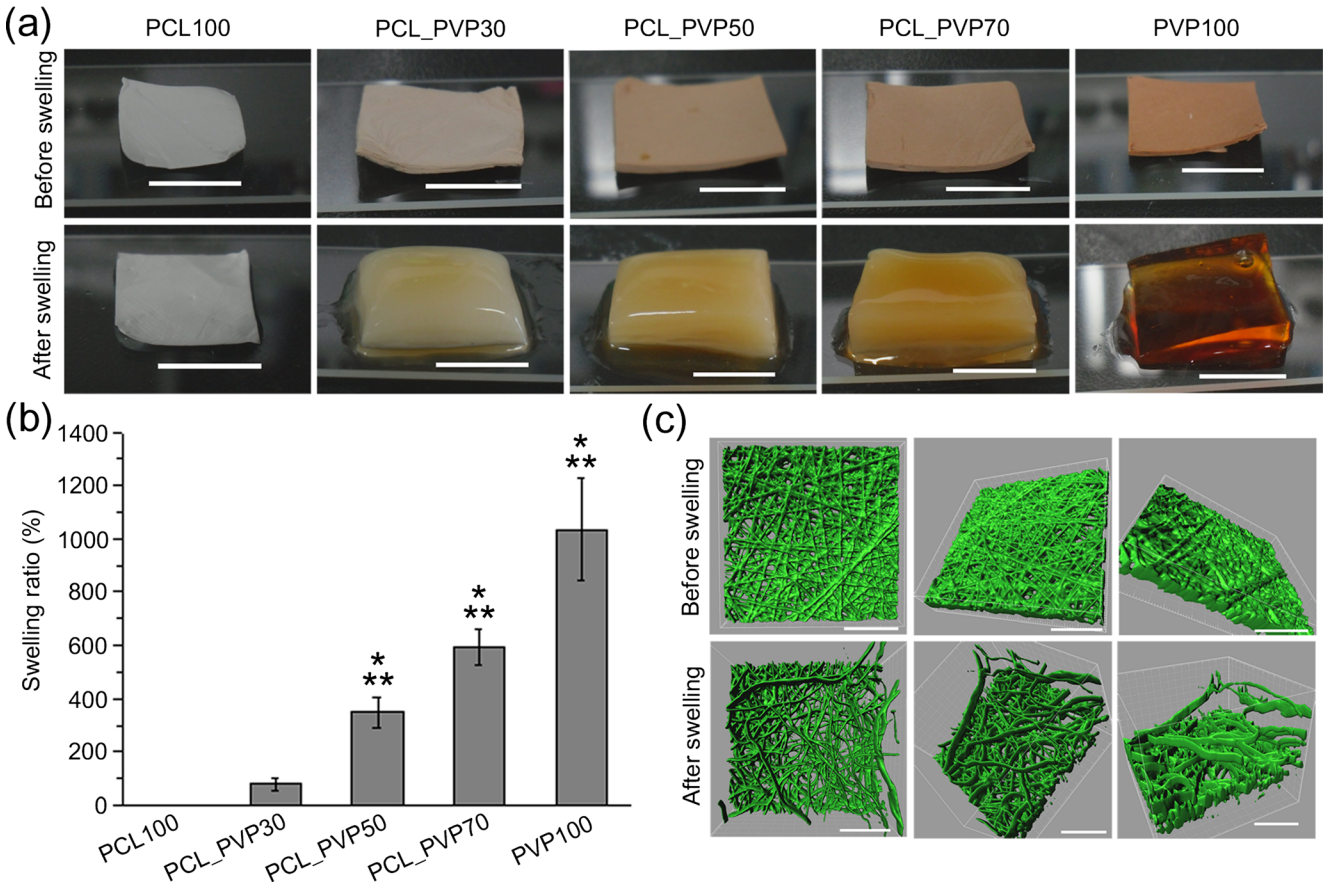

Fig. 2 Morphological changes in the fibrous scaffolds before and after swelling. (**a**) Digital images illustrating the volumetric changes of each scaffold (PCL100, PCL_PVP30, PCL_PVP50, PCL_PVL70, and PVP100). The *scale bar* indicates 1 cm. (**b**) Swelling ratio of each scaffold formulation. The percentage for the swelling ratio was calculated by comparing the increase in thickness after swelling to that before swelling. The symbols * and ** indicate significant differences compared to the swelling ratios of PCL100 and PCL_PVP30, respectively ($P<0.05$). (**c**) Representative z-stacked confocal laser scanning microscopy (CLSM) images of PCL_PVP50 fibers taken before and after swelling. A fluorescent dye (coumarin) was added to the polymer solutions before electrospinning, and the fibrous scaffolds were observed by CLSM before and after swelling. The morphologies of the fluorescent fibers were reconstructed three-dimensionally using Imaris 7.4.2 software. The scale bar represents 100 μm

while maintaining the length and width of the scaffolds, were observed (Fig. 2a).

Compared to PCL-only electrospun scaffolds (*i.e.*, PCL100), large portions of PVP within the scaffolds (*i.e.*, PCL_PVP50, PCL_PVP70, and PVP100) resulted in significant increases in the swelling ratios ($P<0.05$), which were determined by measuring changes in thickness after swelling (Fig. 2b). Slight volumetric changes after immersion in water were observed when the scaffolds were formulated with PCL_PVP30, presumably due to the relatively low amount of PVP in the scaffold. As hypothesized, the substantial volumetric expansions in the electrospun scaffolds appear to be due to the remarkable spatial tortuosity of fibers, likely caused by the hydrogelation of PVP fibers in the moisturized environment. The z-stacked CLSM images of PCL_PVP50 scaffolds, shown in Fig. 2c, clearly confirmed the structural alterations in the electrospun fibers after immersion in water, suggesting the possibility of spatial tortuosity of the hydrogel-hybrid fibers to secure the inner spaces of the scaffold. Regarding the surface morphologies visualized by SEM, all scaffolds possessed straight fibers before swelling, whereas the PVP-containing scaffolds, specifically PCL_PVP50 and PCL_PVP70, exhibited a larger presence of tortuous fibers after swelling (Fig. 3a). No differences were apparent between the fiber morphologies of the flat PCL100 fibrous scaffolds, regardless of the swelling process. Photo-crosslinked PVP chains demonstrated a high equilibrium swelling ratio of 380 % (Ignatova et al. 2007), suggesting that they could spatially kink the relatively rigid PCL fibers. For the PVP100 scaffolds, fibrous structures were observed before swelling, but substantial deformation of the fibrous structure was observed after swelling, resulting in a porous structure typical of hydrogels.

To examine the mechanism behind the volumetric expansion of the PVP-containing scaffolds, the coexistence of the PVP component within the fibrous scaffolds before and after swelling was confirmed by FT-IR spectroscopy (Fig. 3b and c). A characteristic peak for the PCL-only scaffolds was observed ranging from 1725 to 1720 cm^{-1}, which corresponded to the C=O stretch of the ester in the PCL molecule. The amide bonds of the PVP were identified as a stretching vibration of the C=O and were observed at approximately 1,660 cm^{-1}. These characteristic peaks of PCL and PVP were observed for all the PCL-PVP hydrogel-hybrid

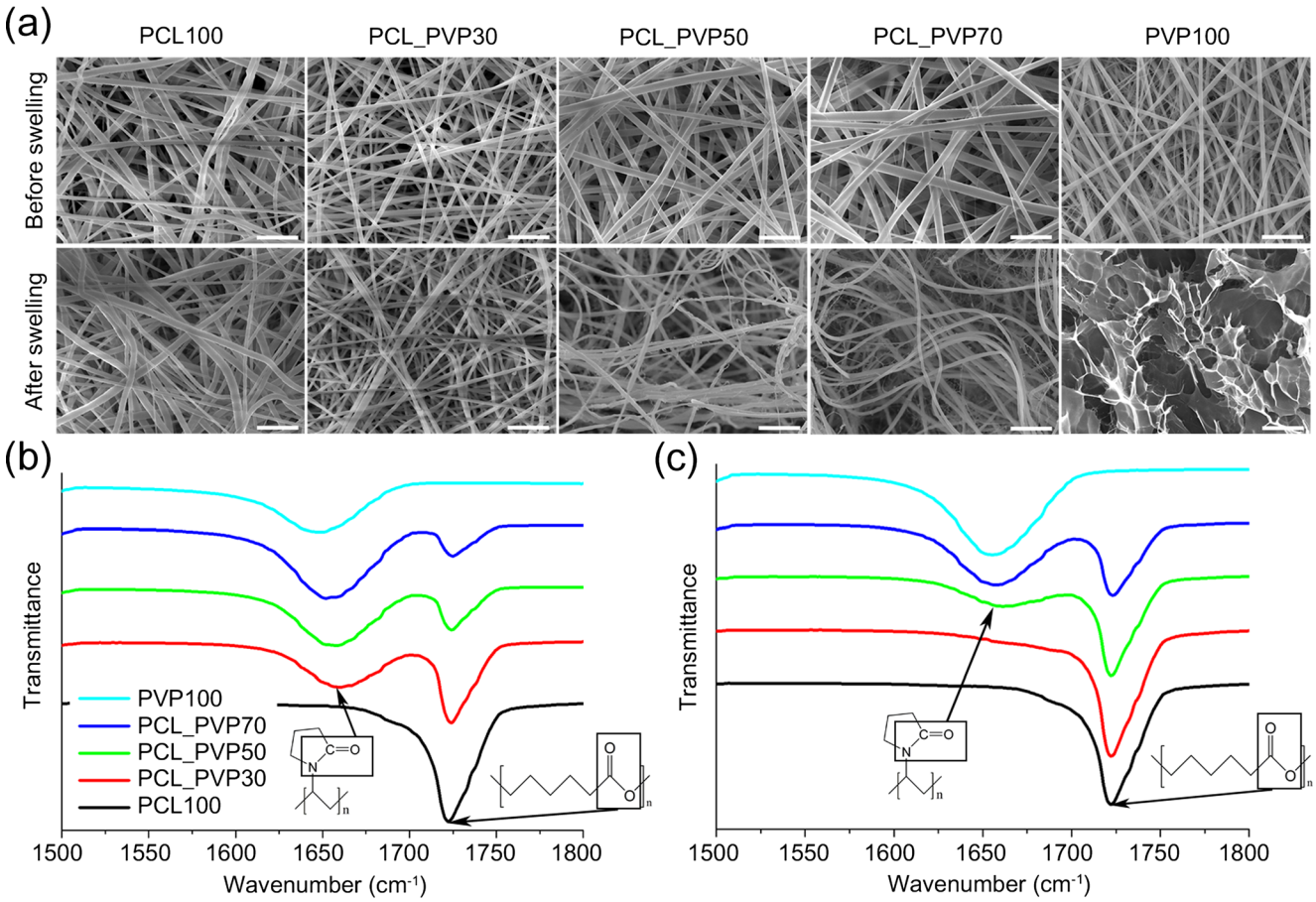

Fig. 3 Physical configuration and chemical composition of the fibrous scaffolds before and after swelling. (**a**) The morphological changes of each scaffold surface (SEM images) before and after swelling. The *scale bar* represents 10 μm. Infrared spectrum of the dual fibers before (**b**) and after (**c**) swelling. The peaks denoted by *arrows* indicate the presence of the C = O bond from the ester of PCL and the amide bonds within PVP

fibrous scaffolds, confirming the coexistence of PVP with PCL fibers after the side-by-side dual electrospinning process (Fig. 3b and c). As the feed rates of the PVP solution increased, which increased the quantity of PVP in the scaffolds, characteristic peaks of PVP emerged, suggesting the existence of additional PVP fibers within the bicomponent scaffold. The characteristic peak of PVP was more obvious before swelling than after, implying the loss of some of the PVP components during the immersion process due to their water-solubility.

To examine the key factors used to increase the volume of the PVP-contained scaffolds, the structures of the individual fibers were characterized by analyzing fluorescence images of dual fibers (Fig. 4 and Online Resource 3). To acquire the fluorescence images, fluorescent dyes were added to the PCL and PVP layers before fiber production, and the structures of the PCL-PVP hydrogel-hybrid fibers before immersion in water were subsequently observed by CLSM (Fig. 4a). The presence of PVP fibers (red color) within the PCL_PVP30 scaffold was rarely observed, which was consistent with the vague characteristic PVP peak within the PCL_PVP30 scaffold in FT-IR analysis (Fig. 3b and c). The majority of existing fibers (PCL_PVP50 and PCL_PVP70) were composed of two different polymers in a single fiber, with a smaller fraction of fibers simply comprising individual materials (Fig. 4 and Online Resource 3). The electrospun hydrogel-hybrid fibers exhibited two common features: PCL-PVP hydrogel-hybrid fibers in which PVP hydrogel layers asymmetrically wrapped the rigid PCL fibers (PCL_PVP50) and PVP fibers aligned in parallel with the PCL fibers (PCL_PVP70) (Fig. 4b and c). The sequential CLSM images taken by sectioning in the z-direction confirmed the dual structures of the hydrogel-hybrid fibers (Fig. 4b and c). Most importantly, the majority of PVP fibers (*i.e.*, PCL-PVP hydrogel-hybrid fibers) after immersion in water still exhibited a fibrous architecture and remained parallel to the PCL fibers (Online Resource 3). Consequently, even after immersion in water, the fibrous structures of the hydrogel-hybrid PCL-PVP scaffolds were maintained within the swollen scaffolds. This result was in stark contrast to the disruptions of fibrous structures in hydrogel scaffolds after swelling that were distinctively observed in previous studies (Thorvaldsson et al. 2013; Tonsomboon and Oyen 2013; Strange et al. 2014). The kinking caused by the spatial fiber tortuosity was not observed within the PVP100 scaffolds because there might be no backbone PCL fibers along with

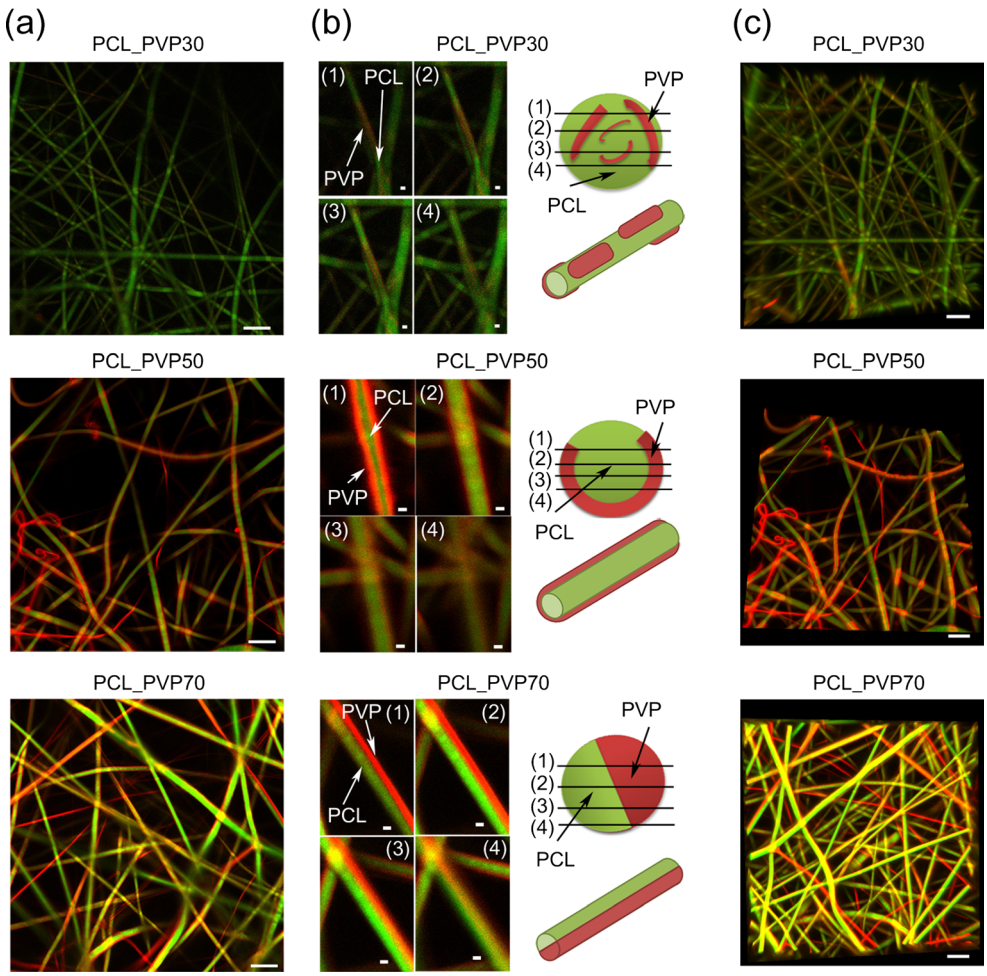

Fig. 4 Structural analysis of PCL-PVP hydrogel-hybrid fibers. (**a**) CLSM images of each fibrous scaffold before swelling. The fluorescent dyes coumarin (*green*) and rhodamine B (*red*) were added to the PCL and PVP solutions before electrospinning, respectively. (**b**) Sequential CLSM images of a randomly chosen fiber, sectioned in the z-direction. (**c**) Three-dimensional z-sectioned CLSM images of each fibrous scaffold. The *scale bar* represents 10 μm (**a**), 1 μm (**b**) and 10 μm (**c**). The right schemes of (**b**) indicate the presumptive cross-section and macroscopic morphologies of representative fibers, which were illustrated based on the sequential images (*i.e.*, (1) – (4))

the PVP fibers. The hydration of a single hydrogel material (*i.e.*, PVP100) resulted in uniform swelling of the electrospun hydrogel fibers followed by the deformation of the fibrous structure. The PCL backbone fibers aligned in parallel with the PVP fibers may prevent the uniform spreading of the swelling forces exerted on the PVP fibers, possibly causing the irregular, spatial tortuosity of the PVP fibers. Taken together, the parallel alignment of PVP with PCL fibers appears to be a key for retaining the fibrous structures, maximizing the spatial tortuosity of the resulting fibers, and ultimately expanding the volume of the flat PCL-PVP mats (Fig. 1a).

The increases in the inner-spaces of the PVP-containing scaffolds corresponded to significant increases in the porosity of the hydrogel-hybrid scaffolds compared to PCL100 scaffolds (Fig. 5a). As the extent of swelling increased, which corresponded to increasing PVP content in the scaffolds, the specific pore volume of the scaffolds, defined as the volume of pores per unit mass of scaffold (Cai et al. 2013), was noticeably increased (Fig. 5a). The swollen PCL_PVP70 scaffolds (89.26±13.96 cm^3/g) exhibited the largest pore volume, exhibiting an approximately 11-fold increase in the pore volume compared to the non-swollen PCL_PVP70 (8.33± 3.04 cm^3/g). In addition, the porosity of the swollen PCL_PVP50 scaffolds (63.86±8.41 cm^3/g) significantly increased compared to the non-swollen PCL_PVP50 (9.82± 1.93 cm^3/g). There were no significant differences between the pore volumes of the conventional PCL-only scaffolds before and after swelling (2.88±0.64 cm^3/g and 3.82± 0.23 cm^3/g, respectively). The pore volumes of the swollen PCL_PVP50 or PCL_PVP70 scaffolds were approximately 20 to 30-fold higher than those of the conventional sheet-like PCL-only fibers, suggesting that the PCL-PVP hydrogel-hybrid fibrous structures could be effective for facilitating cellular ingrowth toward the scaffold interior.

The fiber diameters in the PCL-PVP hydrogel-hybrid fibrous scaffolds were affected by the PVP content of the scaffolds (Fig. 5b). As the PVP content increased within the scaffolds, the diameters of the electrospun fibers gradually increased. Because the fibrous structures of PVP100 scaffolds were lost upon swelling, the fiber diameters in the swollen scaffolds could not be measured. While the diameters of the sheet-like PCL fibers were consistent before and after swelling (1.10±0.43 μm and 1.10±0.48 μm, respectively), significantly reduced fiber diameters were observed after swelling for the PCL-PVP hydrogel-hybrid scaffolds, ranging from 13.1 to 27.8 % ($P<0.01$). The average fiber diameters in the PVP-containing scaffolds (*i.e.*, PCL_PVP30, PCL_PVP50, and PCL_PVP70) after swelling (0.75, 0.98, and 1.05 μm, respectively) were significantly smaller than those before swelling (0.86, 1.27, and 1.45 μm, respectively). The significant reduction in fiber diameters in the swollen PCL-PVP scaffolds compared to the non-swollen scaffolds might be due to the

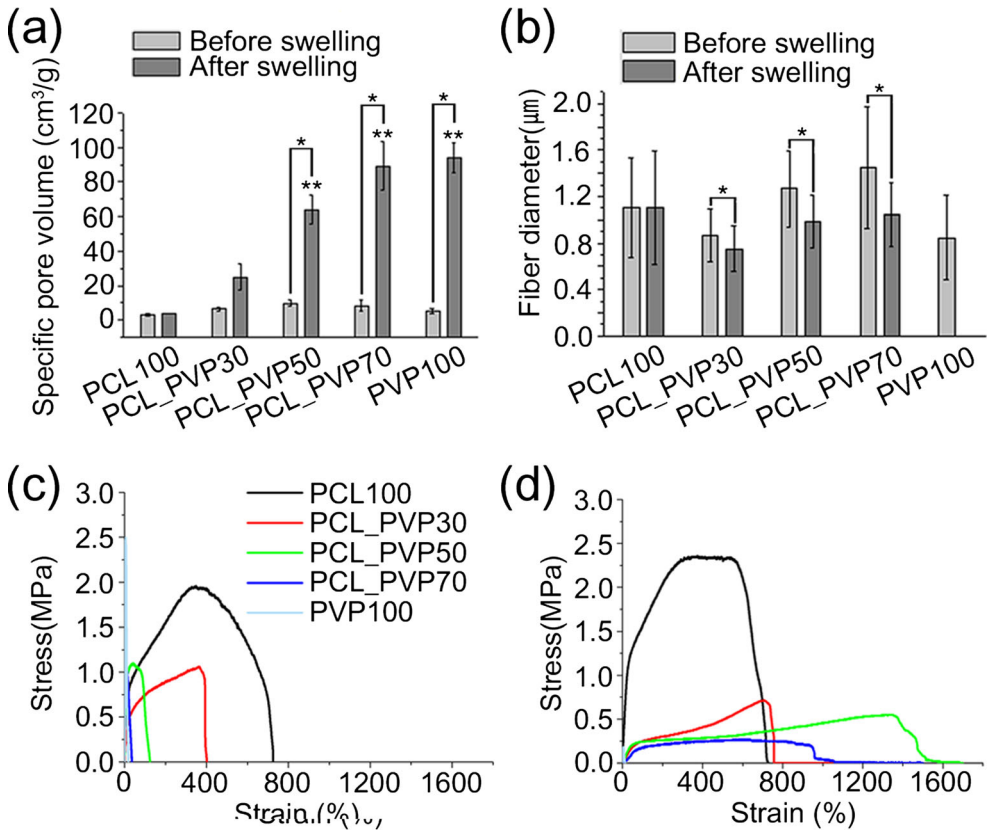

Fig. 5 Physical properties of the hydrogel-hybrid fibrous scaffolds. (**a**) The porosity of the fibrous scaffolds, which was determined by measuring the specific pore volumes. (**b**) Average fiber diameters measured before and after swelling step. The symbol * in (**a**) and (**b**) indicates statistically significant differences ($P<0.01$). The symbol ** in (**a**) indicates significant differences compared to the pore volume of PCL100 after swelling ($P<0.01$). Stress–strain curves of the PCL-PVP fibrous scaffolds before (**c**) and after swelling (d)

loss of small portions of PVP fibers upon immersion in water, presumably due to the water-solubility of PVP (Jiao et al. 2006). Additionally, the parallel elongation of PVP fibers along with the directions of the electrospun fibers might make the dual fibers thinner after swelling. Because the volume of the PCL-PVP hydrogel-hybrid fibrous scaffolds was expanded, even after the diameters of the swollen PVP fibers were reduced, the significant volumetric-expansion upon swelling appears to be caused primarily by the spatial tortuosity of the aligned PCL-PVP hydrogel-hybrid fibers, rather than by the volume change of the PVP fibers themselves.

Importantly, hybridizing the flexible PCL fibers with soft PVP hydrogel fibers elicited ductile properties in the resulting scaffolds (Fig. 5d). Compared to the PCL-only scaffold, the coexistence of PCL-PVP fibers followed by swelling substantially reduced the stress at break (*i.e.*, tensile strength) but increased the ductility of the fibrous scaffolds. The swollen PCL_PVP50 scaffolds demonstrated the highest ductility compared to the other formulations. Swelling did not cause substantial changes in the mechanical properties of the PCL-only scaffolds; the Young's modulus changed from 4.46 to 5.35 MPa, the ultimate tensile strength changed from 2.08 to 2.26 MPa, and the elongation at break changed from 833.74 to 518.67 % (Online Resource 4). However, swelling significantly changed the mechanical properties of the PVP-containing hydrogel-hybrid fibrous scaffolds. Both Young's modulus and the stress at break for the swollen PCL-PVP hydrogel-hybrid fibers, which ranged from 0.47–1.28 to 0.29–0.62 MPa, respectively, were significantly lower than those of the non-swollen hybrid scaffolds (4.82–36.19 and 0.86–1.16 MPa, respectively). The PVP100 scaffolds exhibited no plastic deformation both before and after swelling. However, plastic deformation of the swollen PCL-PVP hydrogel-hybrid fibrous scaffolds occurred under significantly increased strains, and the elongation at break values were 686.48–1295.53 %.

The swollen PCL_PVP50 fibrous scaffolds exhibited the highest plastic deformation and reached a strain of approximately 1295.53 %, illustrating the ductile nature of the hydrogel-hybrid fibrous scaffolds. Interestingly, the swollen PCL_PVP70 fibrous scaffolds demonstrated relatively low strains compared to the swollen PCL_PVP50, suggesting that the mechanical stability of the swollen fibers can potentially be modulated by coordinating the number density of each fiber. Compared to the PCL-only or non-swollen PCL-PVP scaffolds, the reduced moduli of the swollen PCL-PVP hydrogel-hybrid fibrous scaffolds may be ascribed to the decreased volumetric number density of the nanofibers after swelling. Meanwhile, the enhanced strain of the swollen PCL-PVP hydrogel-hybrid fibrous scaffolds might arise from the swelling process itself, as this process might loosen the brittle PVP chains and allow for increased PVP chain mobility. Consequently, the coordinating effect of the flexible PCL fibers with soft swollen PVP chains through dual electrospinning followed by swelling generated the ductile properties of the hydrogel-hybrid fibrous scaffolds. Although the swollen PCL-PVP hydrogel-hybrid fibrous scaffolds exhibited non-rigid features, the mechanical behaviors of the PCL-PVP hydrogel-hybrid fibrous scaffolds were elastic at the lower strain (0~40 %) regimes (Online Resource 4), indicating both the strain-behavior and the modulus values were within the range required for soft tissue regeneration applications, such as skin (Agache et al. 1980) and spinal cord (Tunturi 1980; Ichihara et al. 2001) regeneration.

To evaluate the potential versatility of the swollen three-dimensional fibrous scaffolds for tissue engineering applications, NIH3T3 fibroblast cells were seeded within the scaffolds, and cell viability and infiltration were investigated. The PVP100 scaffold was excluded because the fibrous structures were not maintained after swelling. The metabolic activities of the NIH3T3 cells adhered to the swollen PCL-PVP hydrogel-hybrid fibrous scaffolds at 3 and 7 days post-culture were quantified using a WST-1 assay kit and were not significantly different compared to cells grown on the conventional PCL100 scaffolds or tissue culture plates (Fig. 6a). The average values at the designated time points exhibited slight fluctuations, but there were no significant differences between the conditions.

The volumetric expansion of the fibrous scaffolds provided a favorable environment for cellular spreading and infiltration into the inner space of the scaffolds compared to the two-dimensional PCL-only scaffolds. As shown in the SEM images (Fig. 6b), the majority of cells grown on the PCL-only scaffolds were primarily located on the exterior of the scaffold, whereas the cells cultured on the swollen PCL-PVP hydrogel-hybrid were distributed underneath the fibrous structures. At 7 days post-culture, the presence of cells within the inner space of the swollen PCL-PVP scaffolds was clearly identified compared to 3 days post-culture, suggesting active cell migration toward the scaffold interior. Thus, the increased porosity of the swollen fibrous PCL-PVP scaffolds compared to the sheet-like PCL100 scaffold might result in the improved cellular ingrowth into the scaffold.

Cellular infiltration into the swollen PCL-PVP hydrogel-hybrid fibrous scaffolds was confirmed by H&E staining, which showed cells penetrating the scaffolds under both *in vitro* and *in vivo* conditions. For *in vitro* analysis, scaffolds containing NIH3T3 cells were fixed at 7 days post-culture with 4 % paraformaldehyde (PFA), sectioned to a 16 μm thickness, and stained with H&E. Similar to the results shown in Fig. 6b, most of the cells seeded onto the flat-PCL scaffolds were observed on the exterior surfaces, while a homogeneous cellular distribution was observed when the cells were cultured on the PCL_PVP50 or PCL_PVP70 scaffolds (Fig. 7a). PCL_PVP30, which exhibited the lowest swelling ratio and ductile properties out of the swollen PVP-containing fibrous scaffolds, did not induce uniform cellular distribution across

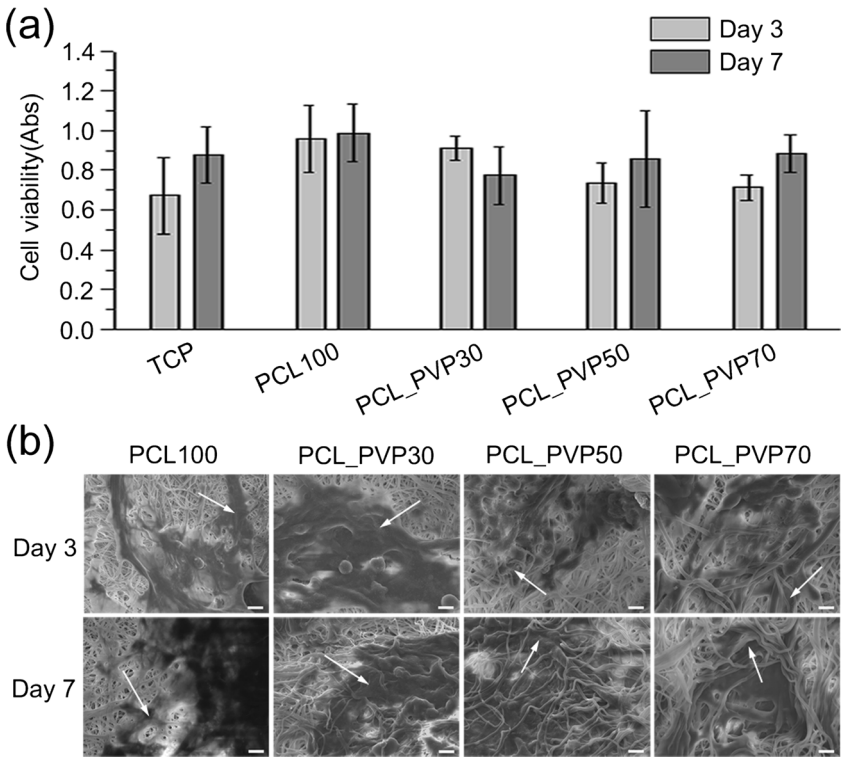

Fig. 6 Viability and attachment of NIH3T3 cells on each fibrous scaffold. (**a**) Cell viability was measured using a WST-1 assay kit at 3 and 7 days post-culture. (**b**) Cellular attachment on the PCL-PVP fibrous scaffolds. SEM images of NIH3T3 cells observed near the exterior surface of each scaffold at 3 and 7 days post-culture. The *arrows* in each panel denote NIH3T3 cells observed near the exterior surface of scaffolds. The *scale bar* represents 10 μm

the scaffold, and the majority of the cells were located near the exterior surface. The non-uniform cellular infiltration of the swollen PCL_PVP30 scaffolds may be attributed to the relatively low portions of PVP within these scaffolds compared to

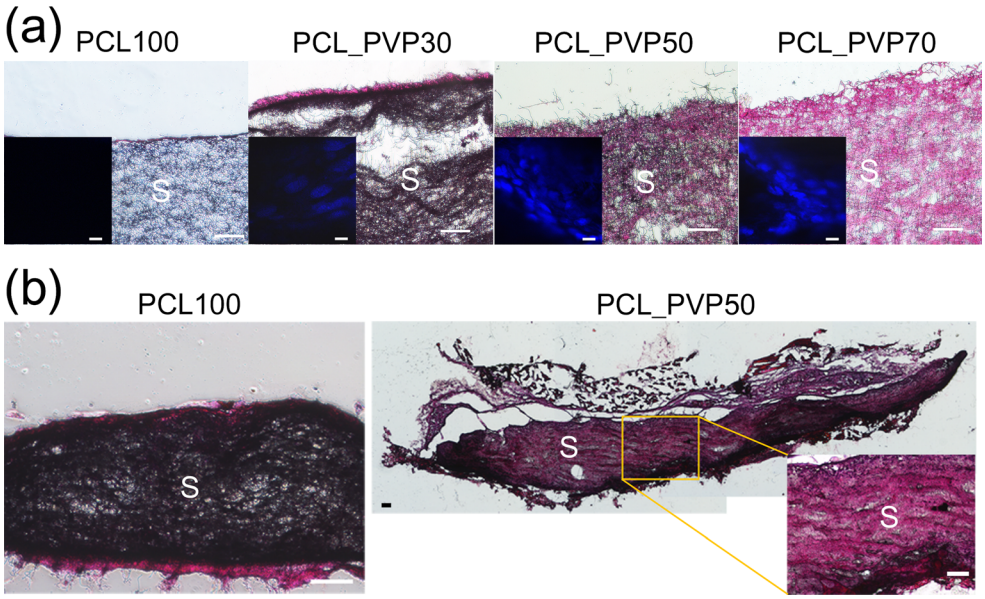

Fig. 7 *In vitro* and *in vivo* performance of the PCL-PVP hydrogel-hybrid fibrous scaffolds. Cellular infiltration across the scaffold was examined to evaluate their performance. (**a**) Histological analysis of the *in vitro* infiltration of NIH3T3 cells at 7 days post-culture. NIH3T3 cells were stained using hematoxylin and eosin (H&E) for observation. The CLSM images demonstrating the nuclei of NIH3T3 cells (blue color; stained with Hoechst dye) within the interior areas of hydrogel-hybrid scaffolds were added as insets. (**b**) *In vivo* cellular infiltration throughout the scaffold. The PCL_PVP50 scaffold, which exhibited the highest ductile properties compared to the other formulations, was implanted subcutaneously into mice and retrieved after 7 days of implantation, after which histological images (H&E) of the scaffolds were taken. For the image of the implanted PCL_PVP50 scaffold, multiple images were assembled to show the entire cross-section of the implanted scaffold. The label 'S' shown in panels denote implanted fibrous scaffolds. The scale bars represent 100 and 10 μm for histological analysis and for CLSM images, respectively

the PCL_PVP50 or PCL_PVP70 groups, which ultimately resulted in a smaller volumetric expansion and lower porosity for PCL_PVP30 (Figs. 2 and 5a). To further convince the enhanced cellular infiltration in the hydrogel-hybrid scaffolds, the nuclei of cells observed within the interior areas of scaffolds were stained using a Hoechst dye, as illustrated in the inset of Fig. 7a. Consequently, large numbers of cell nuclei were visualized in the interior regions of the PCL_PVP50 or PCL_PVP70 scaffolds. These results confirmed the efficient cellular infiltration and validated the H&E staining results.

To further evaluate the tissue engineering potential of swollen three-dimensional PCL-PVP hydrogel-hybrid fibrous scaffolds, PCL_PVP50 scaffolds, which demonstrated the highest ductility and uniform cellular distribution *in vitro*, were subcutaneously implanted into mice and retrieved with adjacent tissues after 7 days. As in the *in vitro* analysis, uniform cellular infiltration was observed throughout the PCL_PVP50 scaffold interior, while the majority of cells were present adjacent to the exterior contour of the sheet-like PCL-only scaffolds (Fig. 7b). The abundance of cells located in the interior of the PCL_PVP50 scaffolds confirmed that the ductile properties of the scaffolds were sufficient to withstand cellular contractile forces during *in vivo* implantation. The improved cellular penetration into the PCL_PVP50 scaffolds may be attributed to the increased inter-fiber spaces, resulting from the curved PCL-PVP fibers produced after swelling. The enhanced ability of the hydrogel-hybrid fibrous scaffolds to promote uniform cellular infiltration with high cell viability and structural integrity confirms their great potential for use in numerous tissue engineering applications, especially for soft tissue regeneration.

4 Conclusions

Dual electrospinning a hydrophobic and a water-soluble material in parallel followed by spatial tortuosity of the crosslinked water-soluble polymer produced highly porous three-dimensional fibrous scaffolds. The ‘spatial fiber tortuosity,’ which is a unique methodology compared to conventional electrospinning techniques typically used to fabricate three-dimensional structures, significantly expanded the volume of the hydrogel-hybrid fibrous scaffolds. Importantly, the post-electrospinning process harmonized the flexible PCL fibers with the soft PVP-hydrogel layers to produce highly ductile fibrous structures. No highly sophisticated apparatus or laborious processing was required for fabricating the three-dimensional fibrous scaffolds. Therefore, due to its simplicity and uniqueness, the ‘spatial fiber tortuosity process’ is a significant technical advancement for tissue engineering scaffold fabrication, which could ultimate facilitate successful transition into clinical trials.

Acknowledgments This work was supported by a National Research Foundation (NRF) funded by the Ministry of Science, ICT & Future Planning (MSIP) through the Active Polymer Center Pattern Integration (No. 2007–0056091), Basic Science Research Program (2012R1A1A1003397) and the Bio & Medical Technology Development Program (NRF-2013M3A9D3046431).

References

P.G. Agache, C. Monneur, J.L. Leveque, J. Rigal, Arch. Dermatol. Res. **269**, 221 (1980)
S. Agarwal, J.H. Wendorff, A. Greiner, Adv. Mater. **21**, 3343 (2009)
B.M. Baker, A.O. Gee, R.B. Metter, A.S. Nathan, R.A. Marklein, J.A. Burdick, R.L. Mauck, Biomaterials **29**, 2348 (2008)
B.A. Blakeney, A. Tambralli, J.M. Anderson, A. Andukuri, D.J. Lim, D.R. Dean, H.W. Jun, Biomaterials **32**, 1583 (2011)
S. Cai, H. Xu, Q. Jiang, Y. Yang, Langmuir **29**, 2311 (2013)
M.-C. Chen, Y.-C. Sun, Y.-H. Chen, Acta Biomater. **9**, 5562 (2013)
L. De Laporte, L.D. Shea, Adv. Drug Delivery Rev. **59**, 292 (2007)
J. Doshi, D.H. Reneker, J. Electrost. **35**, 151 (1995)
A.K. Ekaputra, G.D. Prestwich, S.M. Cool, D.W. Hutmacher, Biomacromolecules **9**, 2097 (2008)
P. Gupta, G.L. Wilkes, Polymer **44**, 6353 (2003)
D. Howard, L.D. Buttery, K.M. Shakesheff, S.J. Roberts, J. Anat. **213**, 66 (2008)
K. Ichihara, T. Taguchi, Y. Shimada, I. Sakuramoto, S. Kawano, S. Kawai, J. Neurotraum. **18**, 361 (2001)
M. Ignatova, N. Manolova, I. Rashkov, Eur. Polym. J. **43**, 1609 (2007)
J.H. Jang, Z. Bengali, T.L. Houchin, L.D. Shea, J Biomed Mater Res A **77**, 50 (2006)
Y. Ji, K. Ghosh, X.Z. Shu, B. Li, J.C. Sokolov, G.D. Prestwich, R.A.F. Clark, M.H. Rafailovich, Biomaterials **27**, 3782 (2006)
Y.T. Jia, X.Y. Zhu, Q.Q. Liu, Adv. Mater. Res. **332–334**, 1330 (2011)
Y. Jiao, Z. Liu, S. Ding, L. Li, C. Zhou, J. Appl. Polym. Sci. **101**, 1515 (2006)
M. Kharaziha, M. Nikkhah, S.-R. Shin, N. Annabi, N. Masoumi, A.K. Gaharwar, G. Camci-Unal, A. Khademhosseini, Biomaterials **34**, 6355 (2013)
C.S. Ki, J.W. Kim, J.H. Hyun, K.H. Lee, M. Hattori, D.K. Rah, Y.H. Park, J. Appl. Polym. Sci. **106**, 3922 (2007)
G. Kim, W. Kim, J. Biomed. Mater. Res., Part B 81B, 104 (2007)
T.G. Kim, H.J. Chung, T.G. Park, Acta Biomater. **4**, 1611 (2008)
H.L. Kim, J.H. Lee, M.H. Lee, B.J. Kwon, J.C. Park, Tissue Eng Part A **18**, 2315 (2012)
G.M. Kim, K.H. Le, S.M. Giannitelli, Y.J. Lee, A. Rainer, M. Trombetta, J. Mater. Sci-Mater. M. **24**, 1425 (2013)
Y.H. Lee, J.H. Lee, I.G. An, C. Kim, D.S. Lee, Y.K. Lee, J.D. Nam, Biomaterials **26**, 3165 (2005)
Y.J. Lee, A. Elosegui-Artola, K.H.T. Le, G.-M. Kim, Cell. Mol. Bioeng. **6**, 482 (2013)
S. Lee, S. Cho, M. Kim, G. Jin, U. Jeong, J.H. Jang, ACS Appl. Mater. Interfaces **6**, 1082 (2014)
M.F. Leong, M.Z. Rasheed, T.C. Lim, K.S. Chian, J. Biomed. Mater. Res., Part A **91**, 231 (2009)
L. Li, Y. Qian, C. Jiang, Y. Lv, W. Liu, L. Zhong, K. Cai, S. Li, L. Yang, Biomaterials **33**, 3428 (2012)
J. Nam, Y. Huang, S. Agarwal, J. Lannutti, Tissue Eng. **13**, 2249 (2007)
D.R. Nisbet, J.S. Forsythe, W. Shen, D.I. Finkelstein, M.K. Horne, J. Biomater. Appl. **24**, 7 (2009)
L. Nivison-Smith, A.S. Weiss, J. Biomed. Mater. Res., Part A **100**, 155 (2012)
Q.P. Pham, U. Sharma, A.G. Mikos, Biomacromolecules **7**, 2796 (2006)

M.C. Phipps, W.C. Clem, J.M. Grunda, G.A. Clines, S.L. Bellis, Biomaterials **33**, 524 (2012)
Y.-J. Ren, S. Zhang, R. Mi, Q. Liu, X. Zeng, M. Rao, A. Hoke, H.-Q. Mao, Acta Biomater. **9**, 7727 (2013)
I. Shabani, V. Haddadi-Asl, E. Seyedjafari, M. Soleimani, Biochem. Biophys. Res. Commun. **423**, 50 (2012)
J.W. Shin, Y.J. Lee, S.J. Heo, S.A. Park, S.H. Kim, Y.J. Kim, D.H. Kim, J. Biomater. Sci. Polym. Ed. **20**, 757 (2009)
D.G. Strange, K. Tonsomboon, M.L. Oyen, J. Mater. Sci-Mater. M. **25**, 681 (2014)
B. Sun, Y.Z. Long, F. Yu, M.M. Li, H.D. Zhang, W.J. Li, T.X. Xu, Nanoscale **4**, 2134 (2012)
H.G. Sundararaghavan, R.B. Metter, J.A. Burdick, Macromol. Biosci. **10**, 265 (2010)
A. Thorvaldsson, H. Stenhamre, P. Gatenholm, P. Walkenström, Biomacromolecules **9**, 1044 (2008)
A. Thorvaldsson, J. Silva-Correia, J.M. Oliveira, R.L. Reis, P. Gatenholm, P. Walkenström, J. Appl. Polym. Sci. **128**, 1158 (2013)
K. Tonsomboon, M.L. Oyen, J. Mech. Behav. Biomed. **21**, 185 (2013)
A.R. Tunturi, Physiol. Chem. Phys. **12**, 373 (1980)
C. Vaquette, J.J. Cooper-White, Acta Biomater. **7**, 2544 (2011)
Y. Wang, B. Wang, G. Wang, T. Yin, Q. Yu, Polym. Bull. **63**, 259 (2009)
B.M. Whited, J.R. Whitney, M.C. Hofmann, Y. Xu, M.N. Rylander, Biomaterials **32**, 2294 (2011)
F. Xu, F.Z. Cui, Y.P. Jiao, Q.Y. Meng, X.P. Wang, X.Y. Cui, J. Mater. Sci. Mater. Med. **20**, 1331 (2009)
J. Xue, B. Feng, R. Zheng, Y. Lu, G. Zhou, W. Liu, Y. Cao, Y. Zhang, W.J. Zhang, Biomaterials **34**, 2624 (2013)
D. Yixiang, T. Yong, S. Liao, C.K. Chan, S. Ramakrishna, Tissue Eng., Part A **14**, 1321 (2008)
C. Zhu, W. Deng, J. Pan, B. Lu, J. Zhang, Q. Su, E. Xie, W. Lan, J. Mater. Sci-Mater. El. **24**, 2287 (2013)